



**HAL**  
open science

## Two photon excited fluorescence and hyper Rayleigh scattering of Protoporphyrin IX

Christian Jonin, Cédric Ray, Estelle Salmon, Pierre Leclerc, Bruno Montcel,  
Laurent Mahieu-Williame, Pierre-François Brevet

► **To cite this version:**

Christian Jonin, Cédric Ray, Estelle Salmon, Pierre Leclerc, Bruno Montcel, et al.. Two photon excited fluorescence and hyper Rayleigh scattering of Protoporphyrin IX. *Journal of Photochemistry and Photobiology A: Chemistry*, 2020, 402, pp.112812. 10.1016/j.jphotochem.2020.112812 . hal-03004727

**HAL Id: hal-03004727**

**<https://hal.science/hal-03004727>**

Submitted on 23 Nov 2020

**HAL** is a multi-disciplinary open access archive for the deposit and dissemination of scientific research documents, whether they are published or not. The documents may come from teaching and research institutions in France or abroad, or from public or private research centers.

L'archive ouverte pluridisciplinaire **HAL**, est destinée au dépôt et à la diffusion de documents scientifiques de niveau recherche, publiés ou non, émanant des établissements d'enseignement et de recherche français ou étrangers, des laboratoires publics ou privés.

# Two photon excited fluorescence and hyper Rayleigh scattering of Protoporphyrin IX

Christian Jonin,<sup>1,\*</sup> Cédric Ray,<sup>1</sup> Estelle Salmon,<sup>1</sup> Pierre Leclerc,<sup>1</sup> Laure Alston,<sup>2</sup> Bruno Montcel,<sup>2</sup> Laurent Mahieu-Williams,<sup>2</sup> Pierre-François Brevet<sup>1</sup>

<sup>1</sup>Institut Lumière Matière, Université de Lyon, UMR 5306 CNRS and Université Claude Bernard Lyon 1, F-69622, Villeurbanne, France

<sup>2</sup>CREATIS, Université de Lyon, Université Lyon1, CNRS UMR5220, INSERM U1044, INSA Lyon, Villeurbanne, France

\* corresponding author: christian.jonin@univ-lyon1.fr

## **Abstract**

The two-photon excited fluorescence (TPEF) cross-section of Protoporphyrin IX (PpIX) in solution is determined at different excitation wavelengths. Maxima observed at 620 and 634 nm are associated with two different forms of PpIX already observed in one-photon excited fluorescence studies. In order to further provide insights into these two forms, first hyperpolarizabilities are also reported for these two forms with corresponding depolarization ratio further demonstrating the existence of specific symmetry differences. The static and the frequency dependent first hyperpolarizability were also calculated using Gaussian 09 and compared to the experimental data. This work shows that PpIX can exhibit two forms that might be targeted in applications like oncology clinical agents.

## Introduction

Porphyrins have been intensively investigated due to their wide range of applications such as for photon capture [1], photodynamic therapy [2,3] or selective catalysis [4]. Moreover, porphyrin-based materials also play substantial roles in biological systems. PpIX is a naturally occurring porphyrin constituent of biological compounds in particular. Hemes, the porphyrin-iron compounds found in hemoglobin, are oxygen transporters [5]. Magnesium-porphyrin complexes, known as chlorophyll, are photoreceptors in green plants [6]. It appears then that some functions involving porphyrins are based on their optical properties. More insights into these PpIX properties can therefore open new applications for porphyrin-based materials. For instance, over the last few years, 5-aminolevulinic acid (5-ALA) induced Protoporphyrin IX (PpIX) fluorescence has been widely used in oncology to guide glioma surgical resection [7, 8]. This technique is based on the standard PpIX fluorescence band appearing with a maximum at 634 nm upon one-photon excitation at 405 nm to benefit from the presence of the high molar extinction coefficient Soret band. However, this technique remains limited by the ability to separate 5-ALA induced PpIX from endogenous fluorophores such as nicotinamide adenine dinucleotide (phosphate) (NAD(P)H), flavine adenine dinucleotide (FAD) or retinoids at low PpIX concentrations [9]. This PpIX fluorescence band is also known to be dependent on the microenvironment, in particular the local pH, leading to different fluorescence spectra and quantum yields [10,11]. Indeed, besides this well-known band, another fluorescence band can be observed with a maximum at 620 nm under specific conditions [7]. Montcel *et al.* have proposed to interpret these two bands, hereafter labeled PpIX620 and PpIX634, as bands corresponding to two different forms of PpIX [7, 12, 13]. The term ‘form’ is here used in this manuscript even though its exact nature is still under debate. These two emission bands are commonly excited through a one-photon excitation [9,14–16]. In this work, we focus on the two-photon excitation of these two emission bands and determine their two-photon

fluorescence cross-sections in aqueous buffer solutions. These two bands are indeed particularly interesting in oncology because their intensity ratio is known to be related to the tumor cells density and to the tissue pathological status[7, 13, 17]. Glioblastoma solid component (GBM, high-grade gliomas) mainly exhibits the 634 nm band whereas the infiltrative component of the GBM and low-grade gliomas exhibit similar intensities for both bands. These two bands are however rather spectrally close to each other, only 14 nm apart, and their full width at half maximum (FWHM) ranges between 20 and 30 nm precluding easy separation. These band characteristics can be subjected to changes as a function of their chemical microenvironment [11]. It is therefore of interest to investigate their TPEF as compared to the one-photon excitation fluorescence (OPEF). In addition, the near-infrared TPEF excited around 800 nm shows a reduction in photo-bleaching as well as in auto-fluorescence in endogenous tissues allowing for a deeper penetration[18]. We show in this work performed in buffered liquid solutions that the two PpIX634 and PpIX620 forms hold different nonlinear optical properties allowing for a clear discrimination of one from the other. These results open the way to the improvement in sensitivity of the technique used in oncology surgery based on PpIX fluorescence for example.

### **Sample preparation**

Solutions were prepared by dissolving PpIX(3,7,12,17-tetramethyl-8,13-divinyl-2,18-porphinedipropionic acid, Sigma Aldrich) as a powder into dimethyl sulfoxide (DMSO) to get a stock solution at a concentration of  $1.78 \times 10^{-3} \text{ mol.L}^{-1}$ . This stock solution was diluted into a phosphate buffered saline solution (PBS) with a pH of 7.2 to reach the desired PpIX concentration. PpIX620 samples were obtained by addition of  $12.5 \text{ mmol.L}^{-1}$  of sodium

hydroxide (NaOH) whereas PpIX634 samples were obtained by addition of 1 mmol.L<sup>-1</sup> of Tween20 surfactant (Sigma Aldrich) as proposed in other studies[19].

Liquid solutions were all contained in fused silica cells. All chemicals were used as received without further purification. All samples were stored in the dark and at low temperature before use. The molecular structure of PpIX is given in Figure 1.

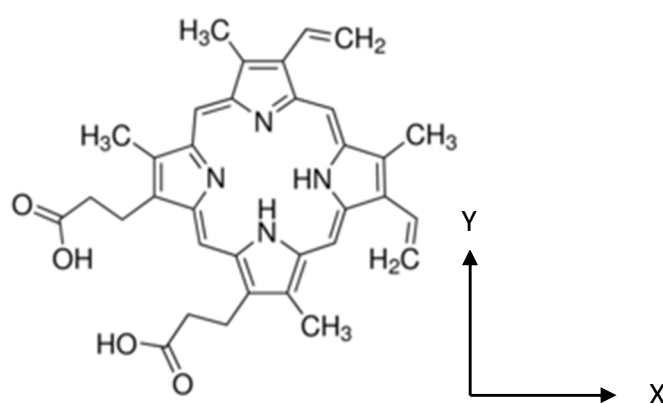


**Figure 1 :** PpIX developed molecular formula.

### Linear optical properties

**Absorption spectra.** The UV-visible absorption spectra of the liquid samples were recorded using a compact spectrophotometer (USB 2000, Ocean Optics). Figure 2 presents the spectra for PpIX620 at three different concentrations. Two distinct absorption bands near 380 nm and between 500 and 750 nm are visible. The band at 380 nm is the common Soret or B band. The second band corresponds to the standard Q bands arising from weaker transitions to the first excited state. The same measurements were performed for the PpIX634 solution and are also shown in Figure 2. The Soret band is also visible albeit with an absorption maximum closer to 405 nm as well as the Q bands in the 500 – 750 nm range. Using concentration dependent

measurements, the extinction coefficients were determined to be  $(60 \times 10^3 \pm 1) \text{ mol}^{-1} \cdot \text{L} \cdot \text{cm}^{-1}$  and  $(114 \times 10^3 \pm 1) \text{ mol}^{-1} \cdot \text{L} \cdot \text{cm}^{-1}$  for the PpIX620 and PpIX634 forms of PpIX respectively, see Figure S1 in Supplementary File.

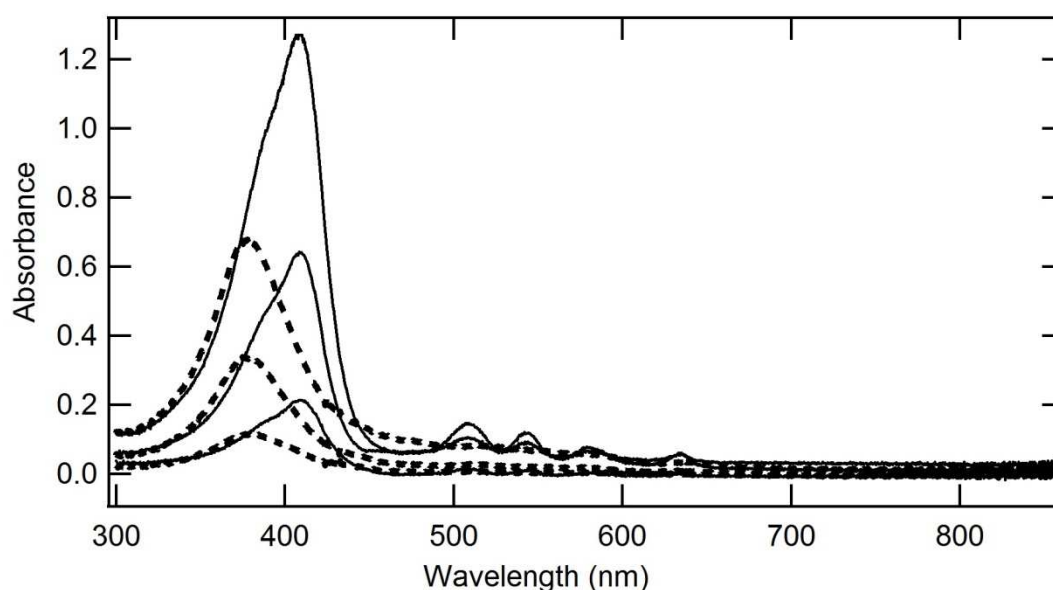


**Figure 2 :**UV-Visible absorption spectra for PpIX634 (full lines) and PpIX620 (dashed lines) aqueous solutions. The solution concentrations are  $2.23 \times 10^{-5} \text{ mol} \cdot \text{L}^{-1}$ ,  $1.15 \times 10^{-5} \text{ mol} \cdot \text{L}^{-1}$  and  $3.35 \times 10^{-6} \text{ mol} \cdot \text{L}^{-1}$  respectively.

**One-photon excitation fluorescence.** Figure 3 presents the normalized OPEF spectra for PpIX in aqueous buffer solution. The excitation wavelength was set at 405 nm and 385 nm respectively for the PpIX620 and PpIX634 forms, in order to be on the absorption maximum in both cases. These spectra are in agreement with the previous studies reported in the literature[20,21]. The PpIX OPEF spectrum exhibits two large bands with maxima around 630 nm and 700 nm. The difference between the two PpIX forms appears as a small shift of about 14 nm between the two main fluorescence bands and a slightly larger one for the two secondary bands.

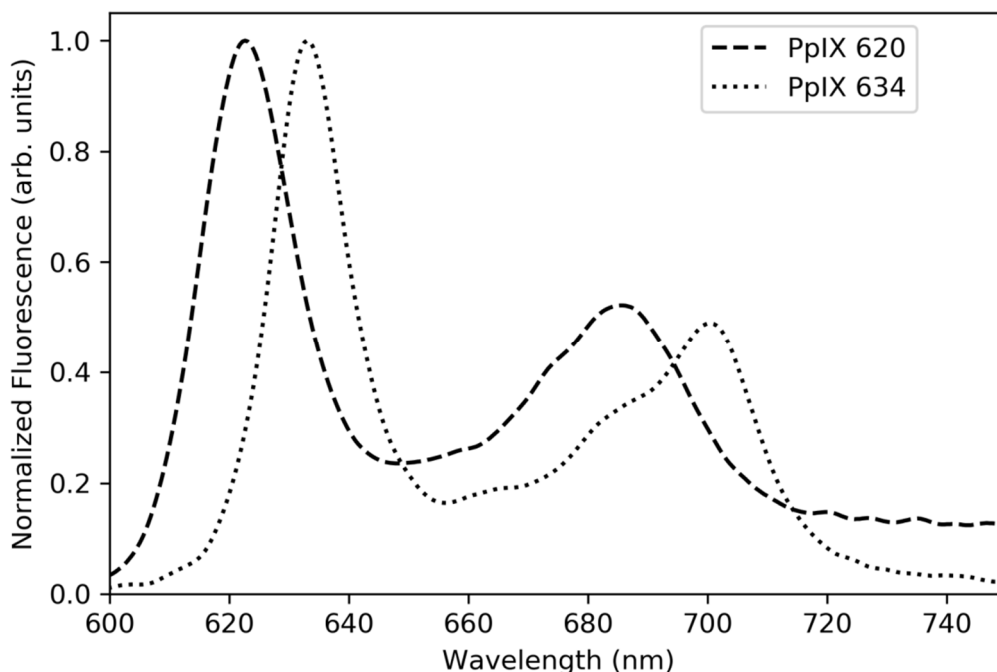


**Figure 3** :OPEF spectra for the PpIX634 (dotted line) andPpIX620 (dashed line) in aqueous solutions. The excitation wavelength is tuned at 405 nm for PpIX634 and 385 nm for PpIX620 respectively in order to match the absorption maxima. The maxima of each spectra are normalized to unity.

### Nonlinear optical properties.

**Two-photon fluorescence.**Figure4 displays the TPEF spectra for the two PpIX620 and PpIX634 forms respectively excited at **785 nm and 804 nm**, the two wavelengths corresponding to twice the absorbance maximum within their experimental control. The maxima of the TPEF intensity for the two PpIX forms are centered at their OPEF maxima. Also, in the PBS buffer solution, the ratio between the TPEF maximum of the PpIX634 and that of the PpIX620 form is about 8 for identical concentrations. **The Maximum of TPEF instensities is 4640 (1s time acquisition) and 58 counts (10s time acquisition) for PpIX634 and PpIX620 respectively.** One of the main features exhibited in Figure4 is the very low overlap of the two fluorescence bands associated with the two PpIX forms ~~as compared to the overlap of their OPEF spectra~~. This point confirms the possibility to better distinguish the two PpIX forms with TPEF

measurements rather than OPEF measurements. The TPEF cross-section  $\sigma$  for the two PpIX forms was then measured by comparing the TPEF spectra obtained in the same conditions with a dye of known cross-section used as reference. Rhodamine-6G (Rh6G) was chosen as the reference due to its stability and high fluorescence quantum yield. **The solvent used to dilute the R6G was the methanol.** The cross-section  $\sigma(\text{Rh6G})$  for Rh6G has been determined to be 60 GM at an excitation around 775-780 nm and 65 GM around 798 – 806 nm. **Its quantum yield is to 0.95** [22]. The TPEF cross-sections were measured at PpIX concentrations of 1.15 mmol.L<sup>-1</sup> at 804 nm and 785 nm and determined using the following expression and the known Rh6G reference values [23]:

$$\sigma_{TPEF}(PpIX) = \frac{F(PpIX)N(Rh6G)}{F(Rh6G)N(PpIX)} \cdot \sigma_{TPEF}(Rh6G)$$

(1)

where  $F(PpIX)$ ,  $F(Rh6G)$  and  $N(PpIX)$ ,  $N(Rh6G)$  are the fluorescence intensities and the concentrations for PpIX and Rh6G respectively. The measured values for  $\sigma(PpIX620)$  and  $\sigma(PpIX634)$  are respectively 0.12 GM at 785 nm and 0.18 GM at 804 nm. **After the index refraction correction these values lead to 0.118 GM at 785 nm and 0.178 GM at 804 nm.** Each cross-section is given at the excitation wavelength close to the absorption maximum for one-photon fluorescence. Therefore, the chosen wavelengths were  $785/2 = 392.5$  nm and  $804/2 = 402$  nm for PpIX620 and PpIX634 respectively. ~~The TPEF cross section obtained for PpIX634 is about ten times smaller to that found by Goyanet al. [24]. They measured values of 0.7 GM, 0.9 GM, 0.6 GM and 2.0 GM for 760 nm, 770 nm, 780 nm and 790 nm excitation respectively. Their measurements only involved the PpIX634 form.~~

One should also compare these TPEF cross-sections with other biological fluorophores. In particular, the TPEF cross-sections are much larger than that of cellular native fluorophores such as flavins or pyridine nucleotides, suitable fluorophores for the 800 nm femtosecond laser source. Indeed, Huang *et al.*[25] have shown that the pyridine nucleotide TPEF cross-section is ten times smaller at 800 nm compared to the two PpIX forms.

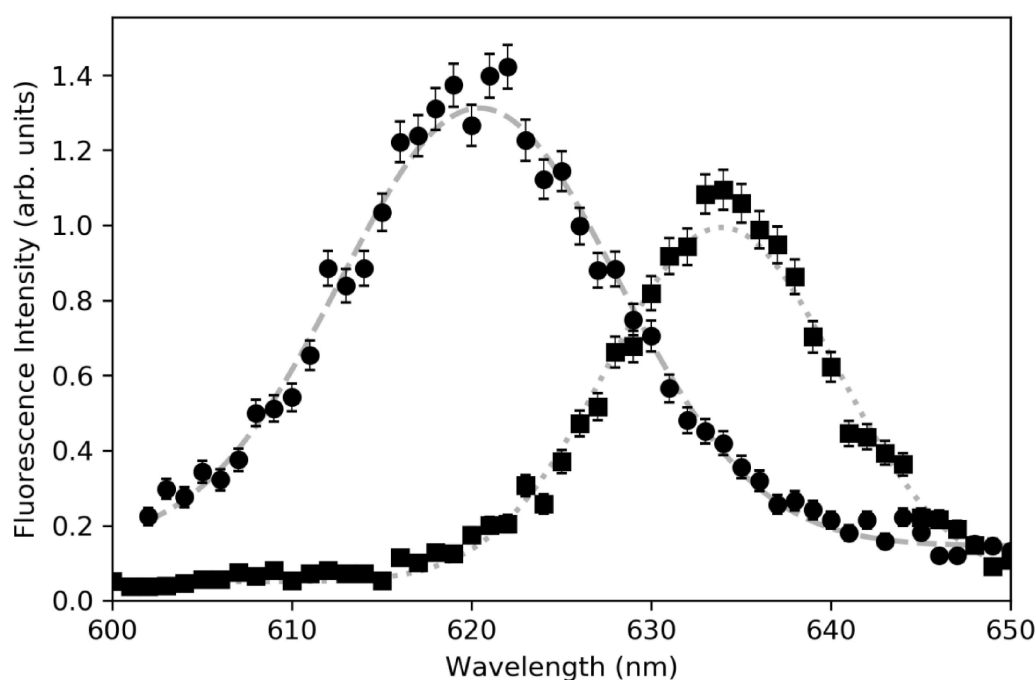


**Figure 4:** Two-Photon-Excited Fluorescence (TPEF) spectra for the PpIX solutions at a concentration of  $1.15 \times 10^{-3} \text{ mol.L}^{-1}$ . The PpIX634 spectrum (squares) is recorded with 1s integration time whereas the PpIX620 spectrum (disks) is recorded with a 10 s integration time. The excitation wavelengths are tuned at 785 nm and 804 nm respectively, in order to be close to the absorption maximum for each species. Dashed and dotted lines correspond to Gaussian adjustments.

**First hyperpolarisability.** Hyper Rayleigh Scattering (HRS) was used to determine the first hyperpolarizability of the two PpIX forms in buffer solutions. The experimental procedure has been described elsewhere[26]. Briefly, a femtosecond Ti: Sapphire oscillator (Verdi pumped

Mira 900, Coherent) delivering pulses with 180 fs duration at 76 MHz was tuned to the fundamental wavelength of 808 nm (FWHM ~5 nm). The incident laser beam was gently focused with a microscope objective (X16, NA 0.25) into the liquid solution. The incident power was controlled with a half-wave plate and a polarizing cube. The harmonic light was collected at right-angle and sent to a photomultiplier tube coupled to a spectrometer. Color filters were placed on the fundamental and the harmonic light beam paths to avoid any unwanted light at fundamental wavelength. Spectra 20 nm in width around the HRS intensity line at 404 nm for both PpIX620 and PpIX634 forms were recorded for various concentrations. This procedure allows us to ensure that the HRS signal is indeed coming from the conversion of two photons at the fundamental frequency into one photon at the harmonic frequency. In addition, the HRS output signal was recorded as a function of the incident power to check that the output signal is proportional to the square of the incident power, see Figure S2 in Supplementary File. In order to determine the first hyperpolarizability of the two PpIXforms, the broadband TPEF background was also subtracted. Figure 5 displays the HRS intensity for different concentrations of the two PpIXforms. The HRS intensity is then adjusted with Eq.(2) [27]:

$$\frac{I_{HRS}^i}{I_{HRS}^{Solvent}} = \frac{\langle N_S \beta_S^2 + N_i \beta_i^2 \rangle}{\langle N_S \beta_S^2 \rangle} = 1 + b N_i \langle \beta_i^2 \rangle \quad (2)$$

where the index  $i$  indicates either the PpIX620 or the PpIX634 form. In Eq.(2),  $N_i$  and  $\langle \beta_i^2 \rangle$  are the number of molecules per unit volume and the square of the first hyperpolarizability averaged over all orientations as expected in a liquid solution for PpIX620 or PpIX634. The parameter  $b = 1/N_S \langle \beta_S^2 \rangle$  in Eq.(2) is the slope of the linear plots where the subscript  $S$  stands for the solvent, the buffer solution in the present case. The hyperpolarizability of the aqueous buffer

solution was first determined and found equal to that of neat water, the value of which is  $\beta_w = (0.087 \pm 0.09) \times 10^{-30}$  esu [28]. The first hyperpolarizability for the two PpIX forms at 808 nm excitation were then found to be  $\beta_{PpIX620} = (67 \pm 6) \times 10^{-30}$  esu and  $\beta_{PpIX634} = (43 \pm 3) \times 10^{-30}$  esu. The origin of this difference in first hyperpolarizability for the two PpIX forms is difficult to assess as the origin can arise from different geometries, electronic and environment properties. Nevertheless, it further demonstrates the possibility to distinguish the two PpIX forms with HRS.

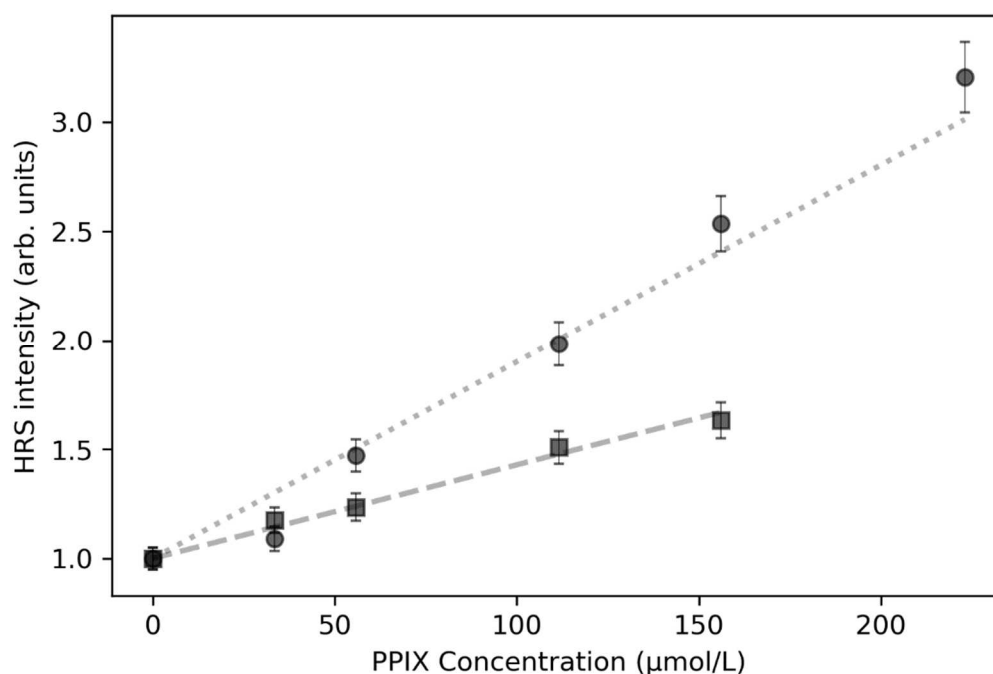


**Figure 5** : Plot of the normalized HRS intensity for PpIX620 (disks) and PpIX634 (square) as a function of concentration. The dotted and dashlines correspond to the linear adjustment to Eq.(2) of the experimental data.

**Theoretical first hyperpolarizability.** In order to get further insights into the PpIX forms, we have also calculated the PpIX first hyperpolarizability theoretically. First of all, the PpIX geometric structure was optimized using the density functional theory (DFT) exchange correlation functional B3LYP in Gaussian 09 and the result is illustrated in Figure 6 where the axis reference frame is indicated with the z axis in blue, the y axis in green and the x axis in

red. It has to be noted in particular that the large aromatic cycle is non-planar and highly distorted. Another view is provided in Figure S3 in Supplementary File.

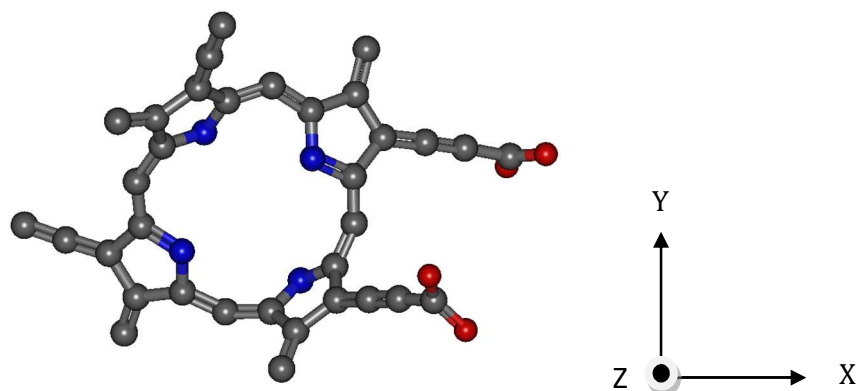


*Figure 6 :Optimized geometry of PpIX and cartesian coordinate system using the DFT exchange correlation functional B3LYP in Gaussian 09 (colours: grey (carbon), red (oxygen), and cyan (nitrogen)) The H atom are not displayed but are taken into account for the calculations.*

We have used the atom-centered split valence with polarization functions 6-311G for C, H, O and N. Hence the static and dynamic polarizability and hyperpolarizability are obtained using Hartree – Fock (HF) level with the 6-311G basis set. The first hyperpolarizability is a 3x3x3 third rank tensor with 27 elements reduced to only 10 components with the Kleinman symmetry [29, 30], e.g. full permutation of the three indices  $\beta_{ijk}$  where  $i, j, k = x, y, z$ . The 10 elements output from Gaussian 09 are listed in Table 1.

**Table 1** :Static hyperpolarizability tensor components in atomic units calculated at HF level using 6-311G basis set by Gaussian09.

$\beta_{xxx}$	$\beta_{xxy}$	$\beta_{yyx}$	$\beta_{yyy}$	$\beta_{xxz}$	$\beta_{yxz}$	$\beta_{yyz}$	$\beta_{zxx}$	$\beta_{zyz}$	$\beta_{zzz}$
-3722	-281	546	2096	354	16.9	996	-672	-705	-264

The main tensor elements are  $\beta_{xxx}$  and  $\beta_{yyy}$ , about ten times the value of the other elements, underlining the close to planar structure of PpIX in the (X,Y) plane. However, coupling with the out-of-plane axis Z is clearly observed with the non-negligible value of the element  $\beta_{yyz}$  as expected from the optimized geometry, see Figure 6. Also, dynamic first hyperpolarizabilities were evaluated at the experimental Ti:Sapphire femtosecond laser wavelength of 800 nm ( $\hbar\omega = 0.057$  a.u.) since the presence of the Soret band enables resonance enhancement at 400 nm. In this case, the Kleinman symmetry breaks down and only the last two indices of the first hyperpolarizability tensor elements permute. Table 2 provides these frequency-dependent first hyperpolarizability tensor elements of PpIX calculated at the CAM-B3LYP/6-31+G\* level.

**Table 2** :Dynamic hyperpolarizability tensor components in atomic units calculated at HF level using 6-311G basis set by Gaussian09.

$\beta_{xxx}$	$\beta_{yxx}$	$\beta_{yyx}$	$\beta_{zxx}$	$\beta_{zyx}$	$\beta_{zzx}$	$\beta_{xxy}$	$\beta_{yxy}$	$\beta_{yyy}$	$\beta_{zxy}$
33400	-3841	234911	-42213	-51272	-62834	5146	28426	-121993	12223
$\beta_{zyy}$	$\beta_{zzy}$	$\beta_{xxz}$	$\beta_{yxz}$	$\beta_{yyz}$	$\beta_{zzz}$	$\beta_{zyz}$	$\beta_{zzz}$		
29304	20918	-8642	5509	69742	-32695	-55747	-97911		

All elements appear resonantly enhanced by a factor of about ten. However, the enhancement is dramatic for the element  $\beta_{yyy}$  which now dominates with the element  $\beta_{yyx}$ . Interestingly, some weak static elements take now rather large values, see for instance the elements  $\beta_{zzz}$  and  $\beta_{zzx}$ . This feature shows how difficult it is to reduce the first hyperpolarizability tensor of PpIX to a reduced set of elements.

**Polarization resolved HRS.** A further insight into the nature of the two PpIX forms can however be obtained with polarization resolved HRS measurements. To this end, HRS intensity was recorded for the two perpendicular output polarization directions, i.e. vertical (V) and horizontal (H) in the laboratory frame, using an analyzer on the harmonic beam as a function of the input polarization angle. The corresponding recorded intensities are denoted  $I_{HRS}^V$  and  $I_{HRS}^H$ . The linear incident polarization was rotated using a half-wave plate on the fundamental beam. The polarization resolved HRS intensities for the two PpIX forms are given in Figure 7.

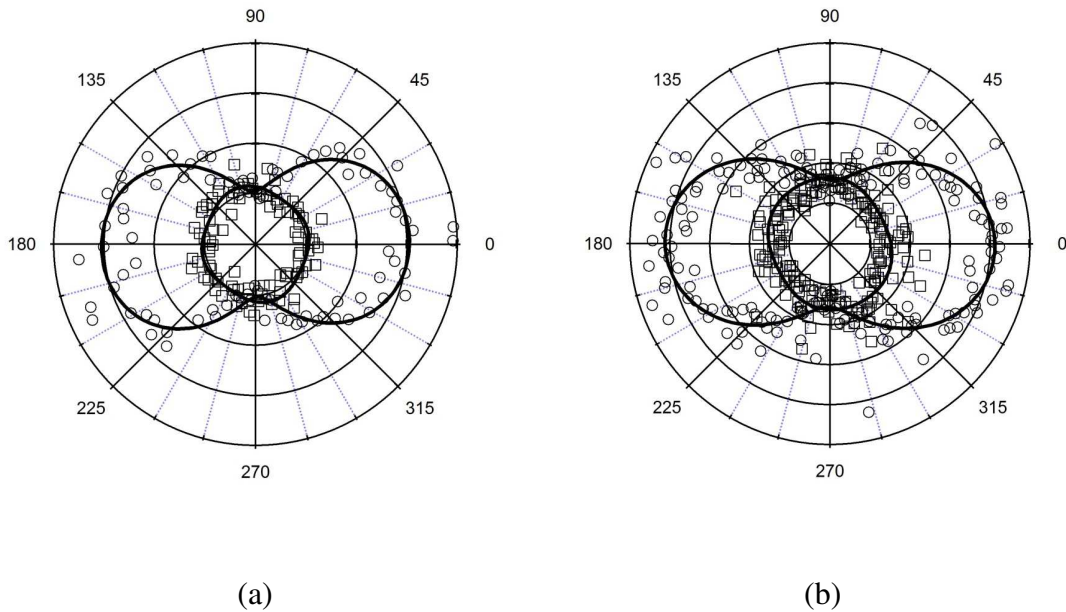


**Figure 7** :Polar graphs of the polarization resolved HRS intensity as a function of the input polarization for (a) PpIX620 and PpIX634 (b). Experimental data recorded in Vertical output polarization configuration (empty circles) and in Horizontal output configuration (empty squares). Full line corresponds to the fit using Eq.(3).

The polarization resolved HRS intensity can be adjusted with a function of the input polarization angle  $\gamma$  with the following equation [31]:

$$I_{HRS}^{\Gamma} = a^{\Gamma} \cos^2 \gamma + c^{\Gamma} \sin^4 \gamma \quad (3)$$

From the adjustments, the depolarization parameter  $D = c^V/a^V$  was determined. This ratio provides information about the molecular symmetry of the two PpIX forms. The values  $D(\text{PpIX620}) = 0.2$  and  $D(\text{PpIX634}) = 0.3$  are obtained. This difference between these two depolarization ratios clearly **suggests** the different molecular structure of the two PpIX forms resulting from small changes in their respective symmetries. The depolarization ratio is defined as

$$D = \frac{\langle \beta_{ZZX} \beta_{ZZX}^* \rangle}{\langle \beta_{XXX} \beta_{XXX}^* \rangle} \quad (4)$$

where the first hyperpolarizability is now given in the laboratory frame using the Z axis as the direction of propagation of the fundamental beam, the Y axis as the scattering direction and the X axis as the vertical polarization axis. The macroscopic averages  $\langle \beta_{IJK} \beta_{LMN}^* \rangle$  were also calculated theoretically using Bersohn *et al.* [32]. In this present work, however, the Kleinmann condition is not fulfilled as observed in Table 2. Therefore, considering all  $\beta_{ijk}$  tensor elements

in the calculation, we obtain a depolarization ratio of  $D = 0.31$ . This result is in very good agreement with the experimental PpIX634 result suggesting that the theoretical first hyperpolarizability given in Tables 1 and 2 rather correspond to the PpIX634 form. Because the structure optimization is performed in vacuum, we note that the environment of the molecule does not play a major role for PpIX634. On the opposite, it appears that the environment induces distortions for the PpIX620 form leading to symmetry changes reinforcing the dipolar component because the experimental depolarization parameter drops from 0.3 down to 0.2.

## Conclusions

We have reported the **relative** TPEF cross-sections and first measurement of the first hyperpolarizability with corresponding depolarization ratio for the two PpIX620 and PpIX634 forms of PpIX. The values measured suggest that the endogenous auto-fluorescence can be neglected in living tissue conditions, an important advantage for the 804 nm excitation TPEF over 400 nm excitation OPEF applications in oncology. These results should be of great help in the future especially for brain biopsies to evidence gliomas infiltrative compounds. In this study, we have also determined experimentally and theoretically the first hyperpolarizabilities for these two PpIX620 and PpIX634 forms. These results also show that these two forms behave differently in HRS and suggest that HRS can also be an alternative to TPEF. Besides, a study of the depolarization ratio shows that the difference between the two PpIX forms may stem from changes in the immediate vicinity of the compound leading to geometry changes or electronic interactions.

## **Acknowledgements**

The authors thank Franck Bertorelle for his help in the sample preparation. This work is supported by the LABEX iMUST [ANR-10-LABX-0064] and the LABEX PRIMES [ANR-11-LABX-0063] of Université de Lyon within the program "Investissements d'Avenir" [ANR-11-IDEX-0007] operated by the French National Research Agency (ANR).

## References

- [1] S. Fukuzumi, *The Porphyrin Handbook*, Academic Press, San Diego, USA, 2000.
- [2] A. M. Battle, Porphyrins, porphyrias, cancer and photodynamic therapy :a model for carcinogenesis,*J. Photochem. Photobiol.B*,20 (1993) 5.
- [3] K. Sugisaki, T. Usui, N. Nishiyama, W.-D. Jang, Y. Yanagi, S. Yamagami, S. Amano, K. Kataoka, Photodynamic therapy for corneal neovascularization using polymeric micelles encapsulating dendrimerporphyrins, *Invest. Ophthalmol. Vis. Sci.*, 49 (2008) 894.
- [4] S. Gharaati, M. Moghadam, S. Tangestaninejad, V. Mirkhani, I. Mohammadpoor-Baltork, B. Barati, F. Sadegh,High-valenttin(IV) porphyrins: Efficient and selective catalysts for cyclopropanation of styrene derivatives with EDA under mild conditions, *J. Organomet. Chem.*, 78 (2013) 741.
- [5] Y.-H. Chen, S.-F. Yet, M. A. Perrella, Role of heme oxygenase-1 in the regulation of blood pressure and cardiac function, *Exp. Biol. Med.*, 228 (2003) 447.
- [6] C. B. Storm, A. H. Corwin, R. R. Arellano, M. Martz, R. Weintraub, Stability constants of magnesium porphyrin-pyridine complexes. Solvent and substituent effects,*J. Am. Chem. Soc.*, 88 (1966) 2525.
- [7] B. Montcel, L. Mahieu-Williame, X. Armoiry, D. Meyronet, J. Guyotat, Two-peaked 5-ALA-induced PpIX fluorescence emission spectrum distinguishes glioblastomas from low grade gliomas and infiltrative component of glioblastomas, *Biomed. Opt. Express.*, 4 (2013) 548.
- [8] R. Weissleder, M. J. Pittet, Imaging in the era of molecular oncology, *Nature*, 452 (2008) 580.
- [9] P.A. Valdés, F. Leblond, A. Kim, B.T. Harris, B.C. Wilson, X. Fan, T.D. Tosteson, A. Hartov, S. Ji, K. Erkmen, N.E. Simmons, K.D. Paulsen, D.W. Roberts, Quantitative

- fluorescence in intracranial tumor: implications for ALA-induced PpIX as an intraoperative biomarker, *J. Neurosurg.*, 115 (2011) 11.
- [10] G.I. Lozovaya, Z. Masinovsky, A. A. Sivash, Protoporphyrin ix as a possible ancient photosensitizer: Spectral and photochemical studies, *Origins Life Evol. Biosphere.*, 20 (1990) 321.
- [11] T.B. Melø, G. Reisaeter, The physicochemical state of protoporphyrin IX in aqueous solution investigated by fluorescence and light scattering, *Biophys. Chem.* 25 (1986) 99.
- [12] L. Alston, D. Rousseau, M. Hébert, L. Mahieu-Williame, B. Montcel, Nonlinear relation between concentration and fluorescence emission of protoporphyrin IX in calibrated phantoms, *J. Biomed. Opt.*, 23 (2018) 097002.
- [13] L. Alston, L. Mahieu-Williame, M. Hebert, P. Kantapareddy, D. Meyronet, D. Rousseau, J. Guyotat, B. Montcel, Spectral complexity of 5-ALA induced PpIX fluorescence in guided surgery: a clinical study towards the discrimination of healthy tissue and margin boundaries in high and low grade gliomas, *Biomed. Opt. Express*, 10 (2019) 2478.
- [14] S. Utsuki, H. Oka, S. Sato, S. Suzuki, S. Shimizu, S. Tanaka, K. Fujii, Possibility of using laser spectroscopy for the intraoperative detection of nonfluorescing brain tumors and the boundaries of brain tumor infiltrates. Technical note, *J. Neurosurg.* 104 (2006) 618.
- [15] N. Haj-Hosseini, J. Richter, S. Andersson-Engels, K. Wårdell, Optical touch pointer for fluorescence guided glioblastoma resection using 5-aminolevulinic acid, *Lasers Surg. Med.* 42 (2010) 9.
- [16] A. Kim, M. Khurana, Y. Moriyama, B.C. Wilson, Quantification of in vivo fluorescence decoupled from the effects of tissue optical properties using fiber-optic spectroscopy measurements, *J. Biomed. Opt.*, 15 (2010) 067006.
- [17] P. Leclerc, C. Ray, L. Mahieu-Williame, L. Alston, C. Frindel, P.F. Brevet, D. Meyronet, J. Guyotat, B. Montcel, D. Rousseau, Machine learning-based prediction of glioma

- margin from 5-ALA induced PpIX fluorescence spectroscopy, *Scientific Reports* 10 (2020) 1462.
- [18] S. Lu, J.-Y. Chen, Y. Zhang, J. Ma, P.-N. Wang, Q. Peng, Fluorescence detection of protoporphyrin IX in living cells: a comparative study on single- and two-photon excitation, *J. Biomed. Opt.* 13 (2008) 024014.
- [19] M. Marois, J. Bravo, S.C. Davis, S.C. Kanick, Characterization and standardization of tissue-simulating protoporphyrin IX optical phantoms, *J. Biomed. Opt.*, 21 (2016) 035003.
- [20] K. König, M.-T. Wyss-Desserich, Y. Tadir, U. Haller, B. Tromberg, M.W. Berns, P. Wyss, Modifications of protoporphyrin IX fluorescence during ALA-based photodynamic therapy of endometriosis, *Med. Laser Appl.*, 21 (2006) 291.
- [21] K.R. Rollakanti, S.C. Kanick, S.C. Davis, B.W. Pogue, E.V. Maytin, Techniques for fluorescence detection of protoporphyrin IX in skin cancers associated with photodynamic therapy, *Phot. Lasers Med.*, 2 (2013) 287.
- [22] N.S. Makarov, M. Drobizhev, A. Rebane, Two-photon absorption standards in the 550–1600 nm excitation wavelength range, *Opt. Express*, 16 (2008) 4029.
- [23] M.A. Albota, C. Xu, W.W. Webb, Two-photon fluorescence excitation cross sections of biomolecular probes from 690 to 960 nm, *Appl. Opt.*, 37 (1998) 7352.
- [24] R. L. Goyan, D. T. Cramb, , **Near-infrared Two-Photon Excitation of Protoporphyrin IX: Photodynamics and Photoproduct Generation**, *Photochem. Photobiol.*, 72 (2000) 821.
- [25] S. Huang, A.A. Heikal, W.W. Webb, Two-Photon Fluorescence Spectroscopy and Microscopy of NAD(P)H and Flavoprotein, *Biophys. J.*, 82 (2002) 2811.
- [26] J. Duboisset, G. Matar, I. Russier-Antoine, E. Benichou, G. Bachelier, Ch. Jonin, D. Ficheux, F. Besson, P.F. Brevet, First Hyperpolarizability of the Natural Aromatic Amino Acids Tryptophan, Tyrosine, and Phenylalanine and the Tripeptide

- Lysine–Tryptophan–Lysine Determined by Hyper-Rayleigh Scattering, *J. Phys. Chem. B*, 114 (2010) 13861.
- [27] K. Clays, A. Persoons, Hyper Rayleigh scattering in solution, *Phys. Rev. Lett.* 66 (1991) 2980.
- [28] J. Duboisset, A. Deniset-Besseau, E. Benichou, I. Russier-Antoine, N. Lascoux, C. Jonin, F. Hache, M.-C. Schanne-Klein, P.-F. Brevet, A bottom-up approach to build the hyperpolarizability of peptides and proteins from their amino acids, *J. Phys. Chem. B*, 117 (2013) 9877.
- [29] R.W. Boyd, *Nonlinear Optics*, Academic Press, New York, 2008.
- [30] D.A. Kleinman, Nonlinear Dielectric Polarization in Optical Media, *Phys. Rev.* 126 (1962) 1977.
- [31] J. Nappa, G. Revillod, I. Russier-Antoine, E. Benichou, Ch. Jonin, P.F. Brevet, Electric Dipole Origin of the Second Harmonic Generation of Small Metallic Particles, *Phys. Rev. B*, 71 (2005) 165407.
- [32] R. Bersohn, Y. H. Pao, H. L. Frisch, Double-Quantum Light Scattering by Molecules, *J. Chem. Phys.* 45 (1966)3184.

Supplementary File

Christian Jonin,<sup>1,\*</sup> Cédric Ray,<sup>1</sup> Estelle Salmon,<sup>1</sup> Pierre Leclerc,<sup>1</sup> Laure Alston,<sup>2</sup> Bruno Montcel,<sup>2</sup> Laurent Mahieu-Williams,<sup>2</sup> Pierre-François Brevet<sup>1</sup>

<sup>1</sup>Institut Lumière Matière, Université de Lyon, UMR 5306 CNRS and Université Claude Bernard Lyon 1, F-69622, Villeurbanne, France

<sup>2</sup>CREATIS, Université de Lyon, Université Lyon1, CNRS UMR5220, INSERM U1044, INSA Lyon, Villeurbanne, France

\* corresponding author: christian.jonin@univ-lyon1.fr

## 1 PpIX Extinction Coefficients

The absorbance was measured for the two PpIX620 and PpIX634 forms as a function of concentration. The resulting graph is given in Figure S1.

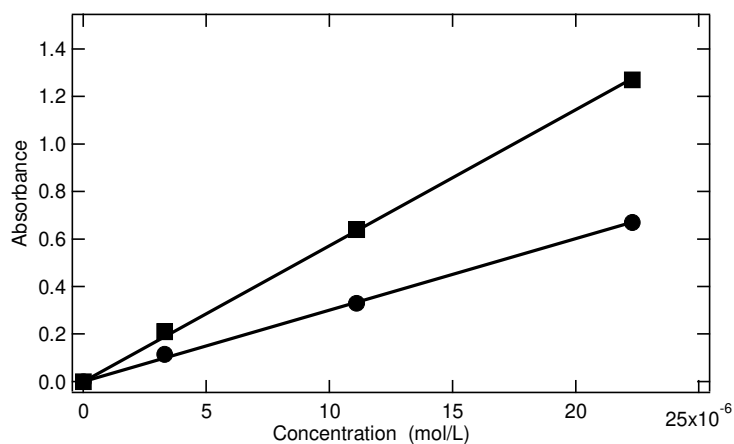


**Figure S1** : Absorbance as a function of concentration for (circles) PpIX620 and (square) PpIX634 aqueous buffer solutions.

The optical path in the absorbance cell was 5 mm. The obtained molar extinction coefficients were found to be  $(60132 \pm 600) \text{ mol}^{-1} \cdot \text{L} \cdot \text{cm}^{-1}$  and  $(114408 \pm 115) \text{ mol}^{-1} \cdot \text{L} \cdot \text{cm}^{-1}$  for the PpIX620 and PpIX634 forms of PpIX.

## 2 PpIX TPEF power dependence

The power dependence of the TPEF observed from the sample was checked for the PpIX634 form. The following graph was obtained.

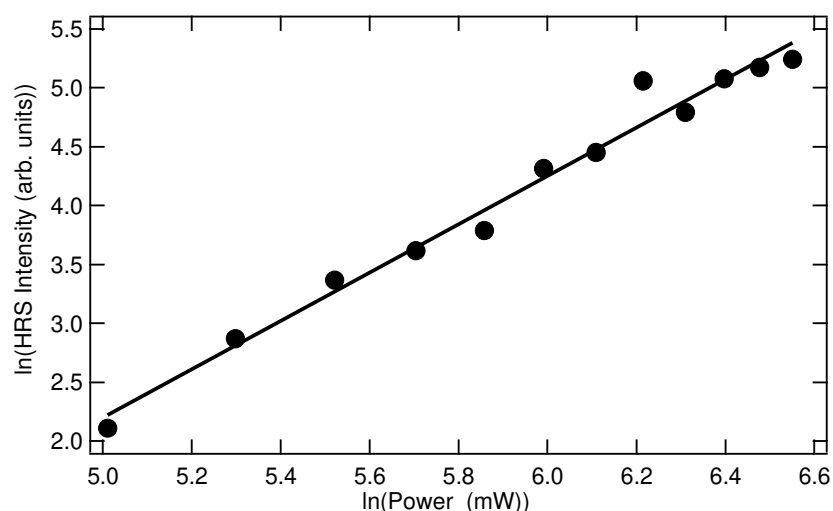


**Figure S2** : Log-log plot of the TPEF intensity collected at its 634 nm maximum as a function of the average power of the exciting fundamental beam for an aqueous buffer solution of the PpIX634 form of PpIX.

A line fit was then performed yielding a slope of (2.05 +/- 0.09), confirming the two-photon excitation nature of the observed TPEF.

## 2 PpIX optimized geometry

In order to show better the non-planar optimized geometry obtained from the Gaussian 09 calculation, see main text, we propose here another view where the direction of sight is going through the aromatic plane.

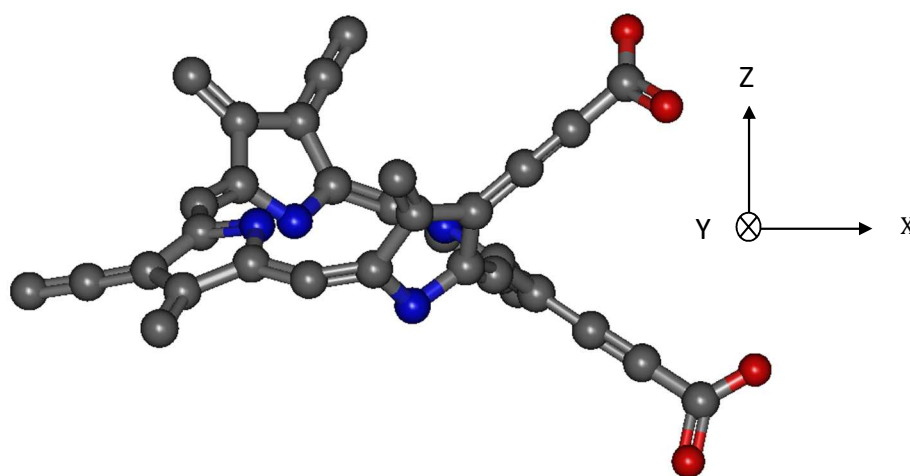


**Figure S3** :Optimized geometry of PpIX and cartesian coordinate system using the DFT exchange correlation functional B3LYP in Gaussian 09 (colours: grey (carbon), red (oxygen), and cyan (nitrogen)). The line of sight is going through the aromatic cycle.

## 3 Experimental setup and TPEF/SHG measurements.

A femtosecond laser (Coherent, model MIRA 900), delivering 180 fs pulses at a repetition rate of 80 MHz, with an average power of at most about 0.5 mW at the sample, was then used to perform the SHG / TPEF measurements. The fundamental wavelength can be tuned around 800 nm for getting the maximum of the absorption for the PpIX620 or PpIX634. The laser beam was then passed through a polarizing cube and a motorized half-wave plate to select the linear input polarization angle, passed through a filter to reject any unwanted harmonic spurious light, and then focused with a 16× objective (Melles Griot, ×16, NA = 0.32). The right angle scattered

SHG light was then sent into the detection line. The latter was constituted with a filter for fundamental light rejection, an analyzer and a lens with focal length  $f = 25$  mm focusing the harmonic beam on the entrance slit of a spectrometer (Spex, model 500M). A CCD camera (Andor, model DU 440) was used as the final detector. By tuning the spectrometer from 370 nm up to 650 nm we get SHG and/or TPEF spectra. The integration of those spectra allow us to get the wanted intensities.

Concerning the SHG resolved polarization measurements, the motorized half-wave plate is moved around its optical axis from 0 to  $180^\circ$  to change the linear input polarization angle then for each input polarization angle the output SHG is collected belong the horizontal axis or the vertical axis by choosing the angle position of the output analyser.